15th IFK
Proc. of the 15th International Fluid Power Conference <Symposium/Conference>
<DOI>

Experimental Comparison of Polymer and Non-Ferrous Metal Slippers for Oil-Hydraulic Axial Piston Machines

Felix Schlegel*[,1], Katharina Schmitz[1]

*[1] institute for fluid power drives and systems, RWTH Aachen, Campus Boulevard 30, 52074 Aachen; *corresponding author: felix.schlegel@ifas.rwth-aachen.de,*

Abstract.

In many hydraulic machines, particularly axial piston units, tribological contacts commonly rely on leaded non-ferrous metal alloys. Increasing legislative restrictions, accelerated oil-aging and copper-corrosion are motivating the search for alternatives. This study demonstrates, using single-piston test rig experiments, that carbon-fiber-reinforced PEEK can replace copper-alloys in the slipper–swashplate contact. It is shown, that polymer slippers show only about 1.3 % lower efficiency than a non-ferrous metal reference but exhibit reduced friction in the mixed lubrication regime. Wear is slightly higher yet remains within the same order of magnitude ($\approx 10^{-10}$ mm^3/Nm), indicating suitability for long-term operation. Wear mechanisms were analyzed using scanning electron microscopy and energy-dispersive X-ray spectroscopy. The results also reveal that polymer deformation significantly influences the effective hydrostatic relief. Variations of several percent with pressure and speed must be considered in polymer slipper design to ensure functional stability.

Keywords. Slipper, Polymer, Friction, Wear, Efficency, lead-free, Axial Piston Machine

1. INTRODUCTION AND STATE OF THE ART

Hydraulic drive systems are widely employed in mobile, industrial, and aerospace applications due to their high power density, controllability, and efficiency. They operate by converting mechanical into hydraulic energy and vice versa, enabling the transmission of large forces and torques within compact systems. Among hydraulic units, axial piston machines (APMs) are the most prevalent design, capable of functioning as both pumps and motors.

The structure of the most common APM type, the swashplate machine is shown in Fig. 1. In pump mode, the drive motor rotates the shaft and cylinder block, moving the pistons, which are pushed outward by the chamber pressure. The inclined swashplate converts this rotation into a reciprocating motion so that fluid is drawn in during the outward stroke and discharged during the return stroke. The stationary valve plate directs the flow to the high-pressure (HP) line during delivery and to the low-pressure (LP) line during suction. In motor mode, the principle reverses when the swashplate is tilted beyond zero in the opposite direction, causing the pistons to be driven outward by pressurized fluid and retracted as the fluid expands. The high hydrostatic forces on the pistons are supported by slippers. Together, the piston–bushing, cylinder block–valve plate and slipper–swashplate interface form the three main tribological contacts determining machine efficiency and lifetime. [X]

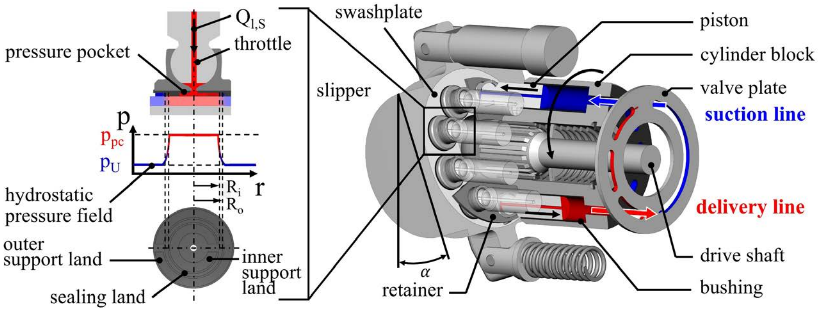

Figure 1.1: Structure of a swashplate type axial piston machine

To enable slippers to follow the swashplate with six degrees of freedom, they are connected to the pistons via spherical joints. This results in complex micro-motions influenced by frictional, centrifugal, and flow forces. This joint may be located on the piston (conventional) or on the slipper (inverse), with the latter allowing larger swashplate angles but leading to less favourable deformation. Because of the high normal loads and the need for operation at low speeds, the slipper–swashplate contact cannot rely solely on hydrodynamic lubrication. A small leakage volume flow from the displacement chambers is routed through bores in piston and slipper to form a hydrostatic pressure field beneath the running surface. There, the un-slitted sealing land defines the hydrostatic pressure drop, achieving 92–105 % load compensation [1, 2]. This hydrostatic relief represents a balance between leakage and friction reduction. Excessive relief may cause lift-off, resulting in leakage, high tilting induced wear or malfunction, which can be prevented by a retainer or, where feasible, an integrated limiting-orifice restricting flow. However, the latter cannot be implemented in all slipper geometries due to manufacturing constraints. Usually, slotted support lands increase slipper stiffness, promote hydrodynamic lift, and reduce local contact pressure. Mechanical slipper failures include joint or neck fracture, whereas tribological failure occurs when wear degrades sealing or alters hydrostatic balance, leading to loss of function.

Afterwards, Sec. 1.1 outlines the calculation of hydrostatic relief, efficiency, and wear of slippers, followed by material selection and the state of research on polymer slippers in Sec. 1.2. The experimental setup and test specimens are described in Sec. 2.1 and 2.2, and the experimental results are presented in Sec 3. Sec 4 provides a critical discussion, followed by Sec 5 concluding with a summary and outlook.

1.1. CALCULATION OF SLIPPERS

This section introduces only the equations required to interpret the results in Sec. 3, details in slipper dynamics are provided in [1]. In general, the hydrostatic pressure field $p(r)$ of a slipper can be described as a potential field along the sealing land radius r with the boundary pressures (pocket p_i, ambient p_a) and the gap height profile $h(r)$, as shown in Eq. (1.1).

$$p(r) = p_i - (p_i - p_a) \cdot \int_{R_i}^{r} \frac{1}{r \cdot h(r)^3} dr \cdot \left(\int_{R_i}^{R_o} \frac{1}{r \cdot h(r)^3} dr \right)^{-1} \tag{1.1}$$

This yields the leakage flow through the annular gap Q as a function of viscosity η and the sealing land geometry defined by inner radius R_i and outer radius R_o (Eq. (1.2)).

$$Q = \frac{\pi}{12\,\eta}\left(\int_{R_i}^{R_o} \frac{1}{r \cdot h(r)^3}\,dr\right)^{-1} (p_i - p_a) \tag{1.2}$$

The hydrostatic force F_S reducing the slipper normal force F_N is obtained by integrating the pocket pressure profile and the sealing land pressure profile, as shown in Eq. (1.3).

$$F_S = \int_0^{Ro} 2\,\pi\, r\, p(r) dr = \underbrace{\int_0^{Ri} 2\,\pi\, r\, p_i\, dr}_{\text{pocket pressure}} + \underbrace{\int_{Ri}^{Ro} 2\,\pi\, r\, p(r)\, dr}_{\text{sealing land}} \tag{1.3}$$

According to Manring [1], this yields Eq. (1.4), and Eq. (1.5) for an even parallel gap.

$$F_{S,even} = p_i\,\frac{\pi(R_o^2 - R_i^2)}{2\ln{(R_o/R_i)}} \quad (1.4) \qquad Q_{even} = \frac{\pi}{6\,\eta}\,\frac{h_G^3}{ln(R_o/R_i)}\,p_i \quad (1.5)$$

Based on this, the static degree of hydrostatic relief B_S can be defined with Eq. (1.6) [1] using the piston force loading the slipper F_P and the swashplate angle α.

$$B_S = F_S \cdot F_P^{-1} \cdot \cos(\alpha) \tag{1.6}$$

Beyond this simple approximation, a logarithmic (Eq. (1.7)) and two polynomial gap profiles of third (Eq. (1.8)) and fifth order (Eq. (1.9)) were studied, representing simulated deformed gaps [3]. The minimum gap height h_o is defined at R_o, and the maximum height h_i at R_i results from deformation (Eq. (1.10)). The scaling factor k (Eq. (1.11)) describes the latter as a function of socket height $H_{S,1}$, layer height $H_{S,2}$, and the young's moduli of socket E_1 and layer E_2. Eqs. 1 and 2 were solved analytically with Eq. (1.7), while Eqs. (1.8) and (1.9) were integrated numerically.

$$h(r) = h_a + \frac{p_i \cdot H_S}{E} \cdot \frac{ln(R_a/r)}{ln(R_a/R_i)} = h_a + k \cdot \frac{ln(R_a/r)}{ln(R_a/R_i)} \tag{1.7}$$

$$h(r) = h_a + k \cdot (8.75\,x^3 - 15.3\,x^2 + 7.12\,x) \tag{1.8}$$

$$h(r) = h_a + k \cdot (3.77\,x^5 - 18.23\,x^4 + 30.32\,x^3 - 20.24\,x^2 + 3.83\,x + 0.78) \tag{1.9}$$

$$h_i = h_a + k \quad (1.10) \qquad k = p_i \cdot \left(\frac{H_{S,1}}{E_1} + \frac{H_{S,2}}{E_2}\right) \quad (1.11) \qquad x = \frac{r - R_i}{R_o - R_i} \quad (1.12)$$

Due to hydrostatic relief, the frictional coefficient μ of a slipper (CoF) cannot be determined from the ratio of friction F_R to normal force F_N (Eq. (1.13)). Instead, the degree of relief must be considered (Eq. (1.14), [1]), making the calculated friction coefficient dependent on the gap-height profile. All CoFs shown below refer to the definition of Eq. 14.

$$\mu = \frac{F_R}{F_N} \quad (1.13) \qquad \mu_S = \frac{F_R}{F_N \cdot (1 - B_S)} \quad (1.14)$$

As slipper design involves a trade-off between friction, leakage, and wear due to hydrostatic relief, it is not useful to compare slippers solely by CoF. For consistent comparison, friction and leakage are evaluated jointly by introducing a slipper efficiency η_{total} (Eq. (1.15), [1]), analogous to APMs, combining hydromechanical η_{hm} and volumetric efficiency η_{vol}.

$$\eta_{total} = \eta_{hm} \cdot \eta_{vol} \tag{1.15}$$

The efficiency definitions applied here differ from those of APMs, as only a single tribological contact is considered. In multi-stage tribosystems, efficiency is defined in series ($\eta_{serial,i}$, Eq. (1.16)), requiring knowledge of both stage losses $P_{loss,i}$ and stage output power $P_{out,i}$. The latter differs from the total machine output power P_{out}, which is reduced by the losses of all stages. As the slipper is isolated here, neither the total input power nor the losses of other stages (e.g., valve plate or piston) are known, rendering this definition inapplicable. Instead, a relative efficiency $\eta_{rel,i}$ is introduced (Eq. (1.17)), referencing stage losses to the total machine output power and thus slightly overestimating efficiency.

$$\eta_{total} = \prod_{i=1}^{n} \eta_{serial,i} = \prod_{i=1}^{n} \frac{P_{out,i}}{P_{in,i}} = \prod_{i=1}^{n} \frac{P_{out,i}}{P_{out,i} + P_{loss,i}} \qquad \text{with: } P_{out,i+1} = P_{out,i} - P_{loss,i+1} \tag{1.16}$$

$$\eta_{rel,i} = \frac{P_{out}}{P_{out} + P_{loss,i}} \quad \text{with: } \eta_{total} \leq \prod_{i=1}^{n} \eta_{rel,i} \tag{1.17}$$

The difference between $\eta_{serial,i}$ and $\eta_{rel,i}$ varies with the stage under consideration. For n identical partial losses, the maximum absolute deviation can be expressed by Eq. (1.18).

$$\Delta\eta_{max}(\eta_{total}) = \eta_{total} - \left(1 + \frac{1}{n}\left(\frac{1}{\eta_{total}} - 1\right)\right)^{-n} \tag{1.18}$$

Pump losses are assumed to be evenly distributed among four tribo-contacts here: slipper–swashplate, piston–cylinder, valve plate–cylinder block, and auxiliary components such as bearings. For total pump efficiencies of 95 %, 90 %, and 85 %, the maximum deviation between relative and serial slipper efficiency amounts to +0.00094 %, +0.0038 %, and +0.0086 %, respectively. This difference is therefore regarded as negligible.

The calculation of individual efficiencies in an APM differs depending on whether it operates in pump or motor mode. In pump mode, η_{hm} is derived from the theoretical drive torque $M_{th,p}$ (Eq. (1.19), [1]), while in motor mode it is based on the effective output torque $M_{th,m}$ (Eq. (1.20), [1]). In pump mode η_{vol} is determined from the effective discharge flow $Q_{th,p}$ (Eq. (1.21), [1]) and in motor operation from the theoretical intake flow $Q_{th,m}$ (Eq. (1.22), [1]). Here, M_l is the friction loss torque and Q_l the hydrostatic leakage flow.

$$\eta_{hm,p} = \frac{M_{th,p}}{M_{th,p} + M_l} \tag{1.19}$$

$$\eta_{hm,m} = \frac{M_{th,m} - M_l}{M_{th,m}} \tag{1.20}$$

$$\eta_{Q,p} = \frac{Q_{th,p} - Q_l}{Q_{th,p}} \tag{1.21}$$

$$\eta_{Q,m} = \frac{Q_{th,m}}{Q_{th,m} + Q_l} \tag{1.22}$$

In both operating modes, M_{th} and Q_{th} are expressed by Eqs. (1.23) [1] and (1.24) [1], based on the pressure difference Δp, displacement volume V, and rotational speed n.

$$M_{th} = \frac{\Delta p \cdot V}{2\pi} \tag{1.23}$$

$$Q_{th} = n \cdot V \tag{1.24}$$

In an APM, slipper losses vary with the rotational angle due to kinematics and commutation. In this study, they are derived from measurement data using Eqs. (1.25) and (1.26), assuming that half of the j slippers operate at low pressure (p_{LP}) and the other half at high pressure (p_{HP}) along the path radius R. The low-pressure level is set to 50 bar, as measurements below this value show reduced quality with the existing test setup.

$$M_l(n,p) = \sum_{j=1}^{k} R \cdot F_{R,j}(n,p_j) = \frac{j}{2} \cdot R \cdot F_R(n,p_{LP}) + \frac{j}{2} \cdot R \cdot F_R(n,p_{HP}) \tag{1.25}$$

$$Q_l(n,p) = \sum_{j=1}^{k} Q_{l,S,j} = \frac{j}{2} \cdot R \cdot Q_{l,S}(n,p_{LP}) + \frac{j}{2} \cdot R \cdot Q_{l,S}(n,p_{HP}) \tag{1.26}$$

In addition to efficiency, slipper wear is evaluated in this study. Therefore, the wear coefficient K_W is calculated according to Eq. (1.27) from the weight loss m_W, with v_r denoting the sliding speed, t the test duration, and ρ the density of the running surface.

$$K_W = \frac{m_W}{F_N \cdot \left(1 - B_{S,even}\right) \cdot\ v_r \cdot t\ \cdot \rho} \tag{1.27}$$

1.2. STATE OF THE ART FOR POLYMER SLIPPERS

Slippers in axial piston machines are typically designed as hard–soft material pairs, combining hardened steel with non-ferrous metals (NFM) such as brass or bronze to ensure run-in capability, particle embedding, and reduced adhesion [4]. However, many conventional alloys contain toxic lead and promote lubricant degradation or corrosion due to copper, motivating research alternative soft materials. High-performance polymers, particularly PEEK-based compounds, are being investigated to address these limitations.

Research on polymer slippers for oil-hydraulic systems remains scarce. Stryczek [5] demonstrated the general feasibility of plastic components in fluid power applications, with performance strongly dependent on design. More comprehensive work exists for water-hydraulic pumps. Rokala [6], Schoemacker [7], Guan et al. [8], and Ni et al. [9] examined polymer slippers in such systems, showing that their lower friction can offset water's poor lubricity. Among tested materials, carbon-fiber-reinforced (CF) PEEK exhibited the most favorable performance. Li et al. [10] compared CF-PEEK against various steels in both "pin-on-disc" and water-hydraulic APM tests, reporting wear coefficients on the order of 10^{-7} mm³/Nm and improved behavior under hydrostatic pressure.

Building on these findings, the authors introduced a "slipper-on-disc" test [11] under oil-hydraulic conditions, revealing substantially lower friction and wear than under dry and water lubricated conditions. The present study extends this work by examining functional sample polymer slippers on a component-level single-piston test bench, to evaluate polymer slipper performance and, if possible, to provide proof of functionality.

2. METHODOLOGY AND EXPERIMENTAL SETUP

The implementation of polymer slippers in this study was preceded by parametric simulations [3], which showed that fully polymer designs deform excessively, preventing a planar load-carrying surface and a defined hydrostatic relief. Therefore, hybrid slippers with a steel socket and a thin polymer running surface were developed. As the ball joint connection could not be manufactured, commercially available NFM-slippers were modified by adapting the steel socket and removing the running layer. For high-resolution optical and gravimetric wear assessment and proper sensor integration, comparatively large slippers were designed with a piston diameter of 25 mm and a base diameter of 34 mm. The pistons originate from a 165 cm³ pump for mobile applications, rated at 450 bar, 3000 rpm, and 326 kW. The test rig for these slippers is described in Section 2.1, the design and manufacturing of the slippers in Section 2.2.

2.1. SINGLE-PISTON TEST RIG

The test rig (Fig. 2.1) represents a single slipper-swashplate contact in inverse kinematics to simplify measurements: the slipper (1) remains stationary while an interchangeable flat disk (2, lapped, 100Cr6) is driven up to 3000 rpm (sliding speed 16.6 m/s) without piston stroke.

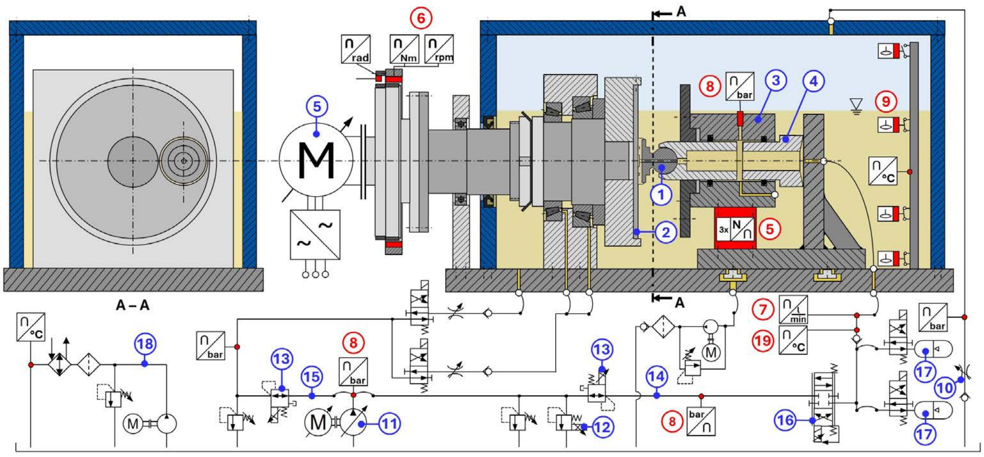

Figure 2.1: Structure of the single-piston polymer-slipper test rig

The slipper is mounted in a piston holder (3) that is axially force-balanced by a compensation piston (4) which is supported on a connecting plate. To enable the measurement of slipper friction with a three-axis force sensor (5, Kistler 9327C, ±8 kN, 0.5 % Full Scale Error (FSE)). A torque measurement shaft (6, Atesteo F1iS, 0-1 kNm, 0-20 krpm,0.03 % FSE, 60 ppr) provides an additional friction reference to validate the measurement principle and enables rotational speed measurement. As the compensating piston setup is inherently leaking and requires the piston holder's center of gravity to coincide with the force sensor centre, a second, sealed holder without force sensor is used to measure hydrostatic leakage flow by a volume flow sensor (7, VSE VS 0.1, 0.01-10 l/min, 0.3 %FSE), whereby the piston pressure is measured in both cases with a pressure sensor (8, Hydac HDA4744, 0-400 bar, 0.25 % FSE). Both holders are aligned by stops and pins for reproducibility. By float switches (9) and a variable throttle (10) in the case drain, the tests can be conducted under different fluid levels and with a controlled case pressure of up to 10 bar.

The hydraulic supply is provided by a pump (11) delivering up to 400 bar at 30 l/min. System pressure is controlled via an electro-proportional pressure valve (12, max. 350 bar), while two pressure-reducing valves (13) allow separate control of the slipper supply (14) and external bearing lubrication (15). A fast servo valve (16) with a step response of 8 ms enables simulation of pump commutation and pulsing of the slipper. Optionally, pump pulsation can be damped with two accumulators depending on pressure (17). The fluid (HLP 46) is conditioned by a circuit (18) including 5 µm filtration, a 30 kW heater, and 40 kW cooling, controlling the slipper inflow temperature at 40 °C (19, Danfoss MBT3270, -50-300 °C, ±1 % FSE). Tests for friction and leakage are fully automated, measuring 30 sec speed ramps up to 3000 rpm at pressures from 0–300 bar in 50 bar increments

For long-term durability tests, the test rig is equipped with superimposed state controllers and enclosed in sound insulation. Surface changes and wear are assessed optically before and after testing using a focus variation microscope (lateral ±0.44 µm, vertical 10 nm) and a confocal profilometer (lateral ±0.5 µm, vertical ±1 µm). Mass loss is determined after ultrasonic cleaning in a class 7/8 DIN EN ISO 14644-1 cleanroom using a class I DIN EN 45501 analytical balance (σ = 0.016 mg).

2.2. POLYMER SLIPPER DESIGN AND MANUFACTURING

The running surfaces of the polymer slippers shown in Fig. 2.2 were machined from rod-extruded PEEK with a melt viscosity of 150 Pa·s at 400 °C (grade 150G). Higher-viscosity grades such as 450G, which offer improved wear resistance, are typically not extruded but could be suitable for mass production by injection molding. All polymer slippers share the same geometry as the NFM reference to ensure direct comparability. The hydrostatic relief degree of the functional samples amounts 92.75 %.

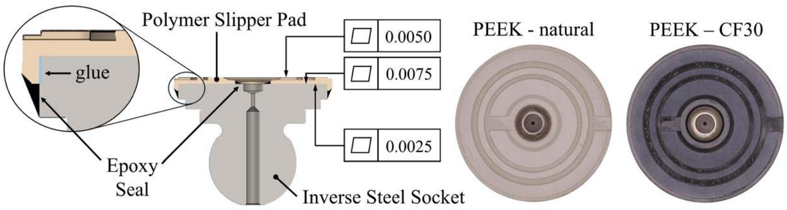

Figure 2.2: Structure of the polymer-slipper functional samples

Besides unfilled 150G PEEK, reinforced variants are tested: 30% carbon fiber (PEEK-CF30) and a composite with 10% carbon fiber, 10% graphite, and 10% PTFE (PEEK-CF10-GR10-PTFE10, HPV). After machining, the slippers were lapped, as surface finish significantly affects wear [11]. A critical challenge for the design investigated here is the tolerance chain involving flatness of the steel base and both pad surfaces. The achieved flatness, shown for the worst case in Fig. 2.2, remained below that of industrially grinded slippers. To avoid changing running surface flatness, the pads were glued only between the pad overhang and the socket outer diameter. The gap between both is sealed with epoxy resin to prevent detachment under pocket and case drain pressure. These steps were required only for the functional samples here, in industrial implementation, overmolding the steel base would enable higher flatness without the need of bonding or sealing.

3. EXPERIMENTAL RESULTS

This section first presents experimental results friction, leakage and efficiency of the polymer slippers in Sec. 3.1, followed by the evaluation of wear in Sec. 3.2.

3.1. FRICTION, LEAKAGE and EFFICIENCY

To evaluate friction and efficiency, the compensation-piston measurement principle introduced in Sec. 2.1 was first validated. Therefore Fig. 3.1 shows friction results of the commercial NFM reference slipper for acceleration (up, 0–3000 rpm) and deceleration (down, 3000–0 rpm) ramps, measured with both the force and the torque sensor. All shown data of this NFM slipper serve only as a reference within the observed conditions. Since material and surface finish of the disc differ, the presented results do not represent the commercial tribosystem. Tests were performed with the housing drained to eliminate flow-induced forces. The bearing friction of the test rig was characterized as a function of pressure and speed and subtracted from the torque data. The good qualitative and quantitative agreement between both methods confirms that the friction of the compensating piston is negligible.

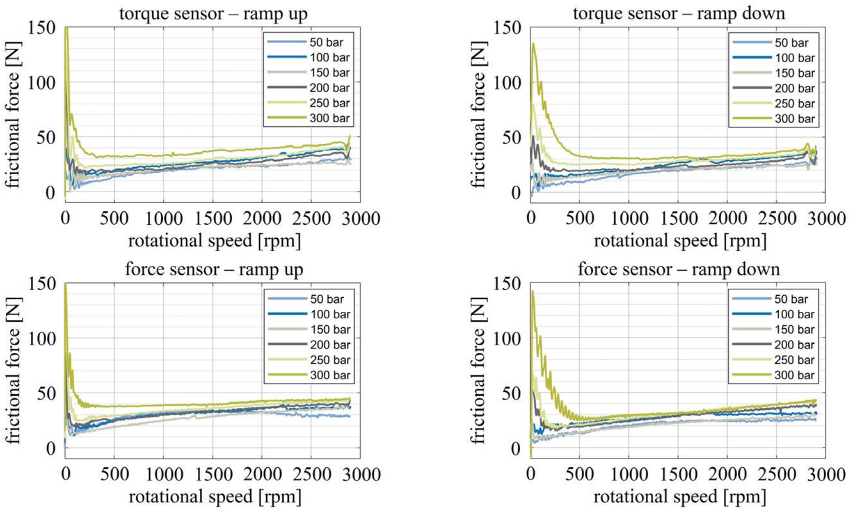

Figure 3.1: Comparison of friction measurements for non-ferrous metal

All curves in Fig. 3.1 show typical Stribeck behavior. During acceleration, the transition from mixed to full-film lubrication (release point) shifts with pressure from about 75 rpm at 50 bar to 250 rpm at 300 bar, consistent with previous findings [12]. A sensor-independent hysteresis is observed, where the difference between acceleration and deceleration at standstill represents static friction. This increases proportional with pressure up to 57 N at 250 bar and decreases afterwards to 16 N at 300 bar. In the mixed lubrication regime, the curves deviate due to hysteresis, leading to the release point occurring at higher speeds (≈450 rpm at 300 bar) during deceleration. As the NFM exhibits no significant viscoelasticity, the hysteresis is attributed to micro-motions of the slipper rather than material damping.

Fig. 3.2 compares the friction behavior of the NFM reference slipper with that of the polymer slipper functional samples during acceleration ramps. The natural PEEK slipper exhibits a distinctly different behavior compared to the reinforced variants. One reason is its poor machinability, which results in inferior surface flatness and sealing, leading to a significant increase in fluid friction. Additional contributing factors are discussed in Sec. 4. All polymer slippers show a pronounced pressure-dependent friction behavior, with a release point occurring below 100 rpm. At low speeds, the PEEK-CF30 slipper exhibits up to 43 % lower friction compared to the NFM reference. In the full-film lubrication regime, however, its friction partially exceeds that of the NFM reference by up to 48 %.

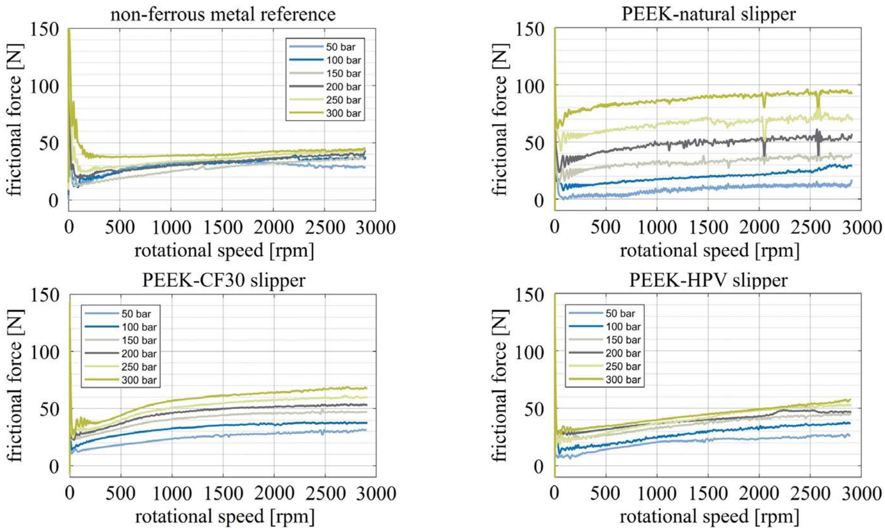

Figure 3.2: Friction comparison of the polymer slipper functional samples

Fig. 3.3 shows a comparison of slipper leakages. The measured leakage represents a superposition of the slipper–swashplate and ball-joint contact leakages. As all slippers were manufactured using pistons from the same production batch, the data is considered comparable.

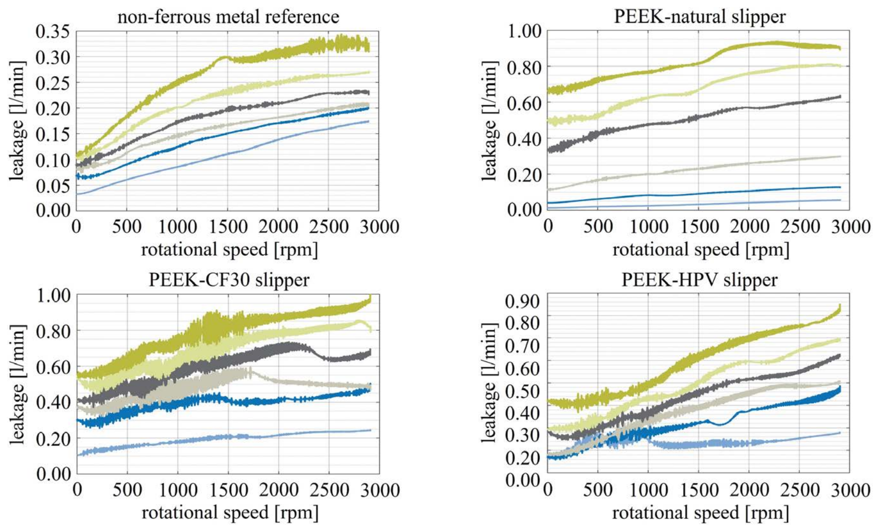

Figure 3.3: Leakage comparison of the polymer-slipper functional samples

The data shown is only lightly filtered, as leakage noise increased with pressure. A minor hysteresis between acceleration and deceleration was observed at low speeds too, with leakage being up to 10 % higher during deceleration but returning to the same value at standstill. Repeated tests revealed a reproducibility band of about ± 8 % for all slippers, including the

NFM reference. It is visible that at lower pressures, leakage increases almost linearly, while at higher pressures it tends to saturate. As expected from the limited flatness described in Sec. 2.2, the NFM reference exhibited the lowest leakage. However, the stronger pressure dependence of the polymer slippers suggests additional effects, discussed in Sec. 4. For the PEEK-CF30 slipper, leakage exceeded the NFM reference by about 26 % at 50 bar and 185 % at 300 bar, yet absolute values remain small compared to the pump's delivery flow (max. 495 l/min). That's why the resulting relative efficiencies are discussed in Fig. 3.4 using the equations from Sec. 1.1.

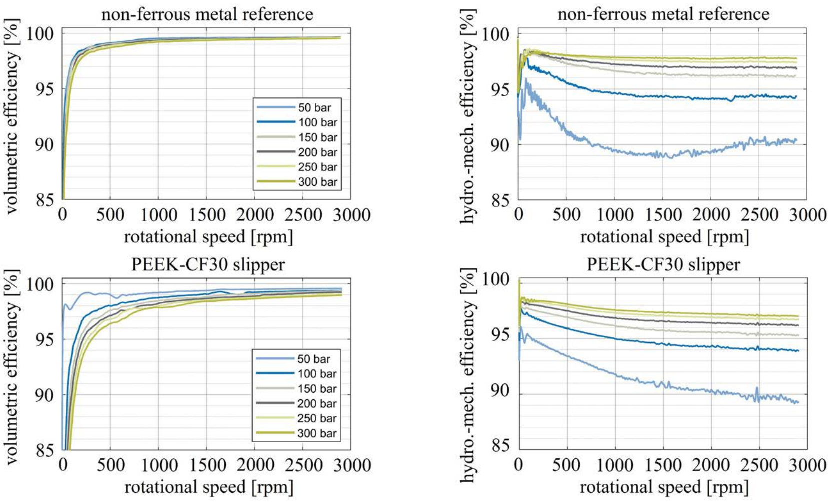

Figure 3.4: Comparison of volumetric and hydromechanical efficiencies

In addition to the partial efficiencies shown in Fig. 3.4, Fig. 3.5 presents a comparison of overall efficiency maps for all tested slippers.

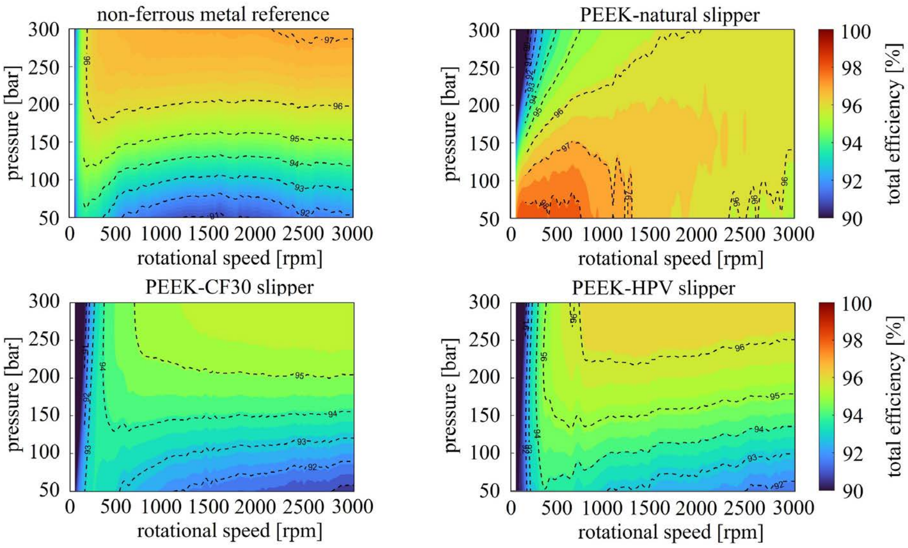

Figure 3.5: Comparison of total efficiencies

The volumetric and hydromechanical efficiencies exhibit the typical trends reported in the literature [1, 2]. Due to lower friction at low speeds, η_{hm} is higher for the polymer slippers, decreasing at higher speeds. However, η_{vol} reveals the stronger pressure dependence and increased leakage, resulting in lower overall efficiency.

The commercial pump is specified with a minimum operating speed of 400 rpm, consistent with the mixed lubrication regime and reduced total efficiency observed in this range. The recommended operating range is 1400–2200 rpm and 230–320 bar, where the overall efficiencies of the PEEK-CF30, PEEK-HPV, and natural PEEK slippers reach approximately 95.4 %, 96.1 %, and 96.2 %, respectively, being only slightly below NFM with 96.7 %.

3.2. WEAR

To assess wear behavior, the mass loss was first determined after 100 h of testing at 1450 rpm and 200 bar to evaluate the general material suitability. Due to the low density of polymers (PEEK-CF30 1.4 g/cm³ vs. NFM 8.1 g/cm³), shorter tests would not allow gravimetric resolution. Fig. 3.6 presents a boxplot with the resulting wear coefficients (Eq. 1.27) together with the friction coefficients over the entire speed range.

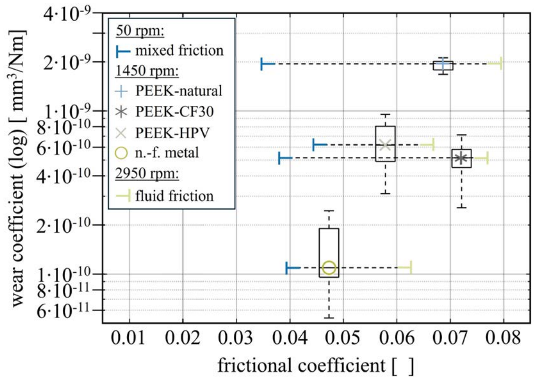

Figure 3.6: Gravimetric wear comparison after 100 h at 200 bar and 1450 rpm

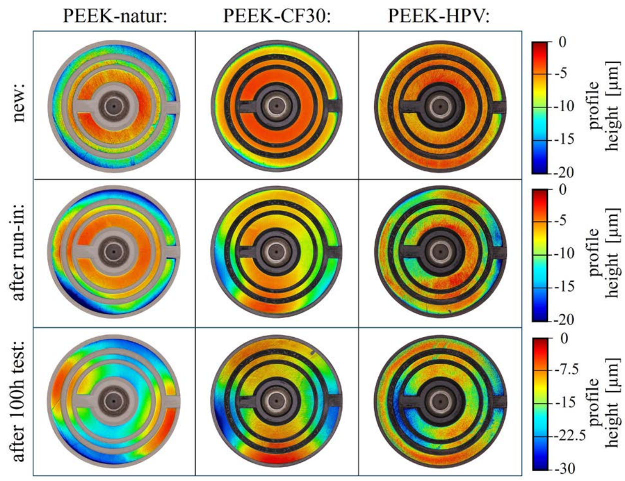

Figure 3.7: Optical wear comparison after 100 h at 200 bar and 1450 rpm

PEEK-CF30 and PEEK-HPV show wear coefficients in the same order of magnitude as NFM (< 10^{-9} mm³/Nm), typical for fully fluid-lubrication and suitable for long-lifetimes. On average, PEEK-CF30 exhibits roughly five-times higher wear, though the scatter indicates that gravimetrical evaluation mainly provides order-of-magnitude estimate in this wear range. In contrast, natural PEEK displays substantially higher wear and is deemed unsuitable. Accordingly, reinforced PEEK is generally suitable, though local wear at the sealing land may still limit durability. Therefore Fig. 3.7 presents optical wear localization.

The top of Fig. 3.7 shows the pronounced non-flatness of new slippers, especially for natural PEEK. Below it is evident that the local wear pattern forms mainly during the 30 min run-in procedure covering the entire operational range, with only quantitative changes thereafter. Wear concentrates near the pressure-relief grooves due to local deformation and stiffness loss, causing groove depression and partial wear transfer onto the sealing land. This may increase leakage or collapse hydrostatic relief over time. Therefore, polymer deformation necessitates geometric compensation as demonstrated in [3], meaning the NFM geometry cannot be directly adopted.

To identify the dominant wear mechanisms, scanning electron microscopy (SEM) and energy-dispersive X-ray spectroscopy (EDX) were performed before and after testing. The aim was to exclude thermal or chemical degradation and to determine whether the polymers form the thin transfer film, typically being responsible for the low wear of tribologically optimized polymers, even under the prevalent high gaps, hydrostatic relief, and smooth surfaces. Figs. 3.9–3.11 show the SEM images, and Figs. 3.12–3.14 the EDX spectra.

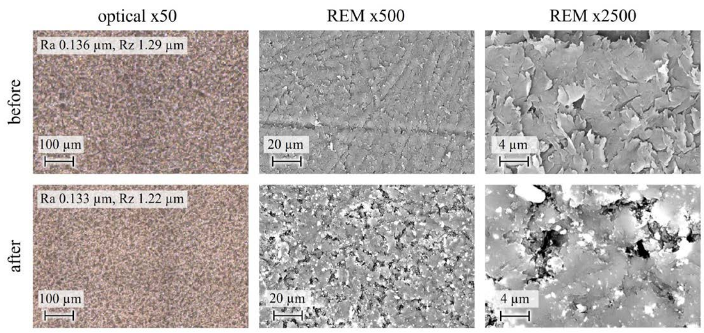

Figure 3.8: PEEK-natural surface before and after wear test

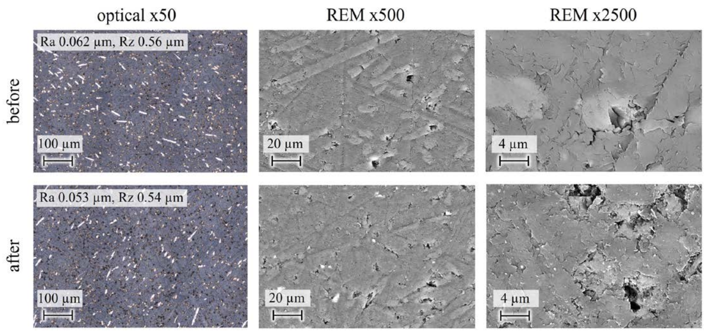

Figure 3.9: PEEK-CF30 surface before and after wear test

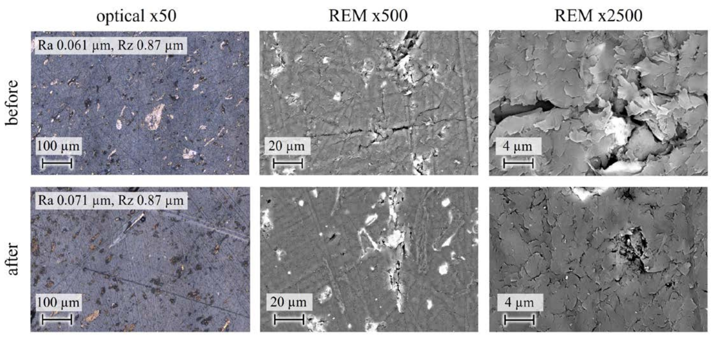

Figure 3.10: PEEK-HPV surface before and after wear test

The SEM images at 2500× magnification reveal surface smoothing for all polymers, with abrasion as the dominant wear mechanism and occasional fiber pull-out in reinforced grades. No signs of melting, structural damage, or chemical attack were detected.

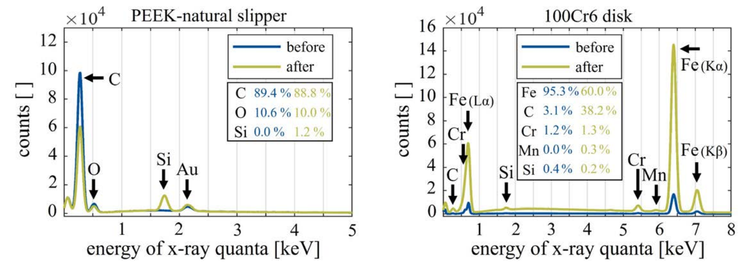

Figure 3.11: EDX-spectra of the PEEK-natural slipper and counter disc

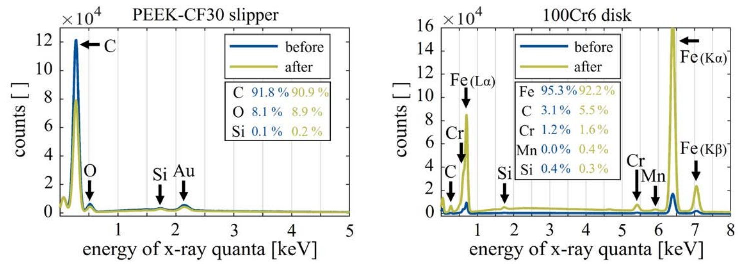

Figure 3.12: EDX-spectra of the PEEK-CF30 slipper and counter disk

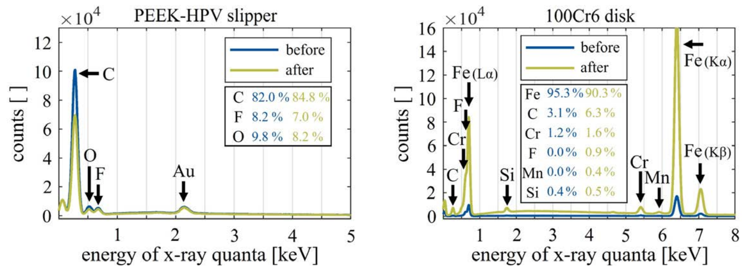

Figure 3.13: EDX-spectra of the PEEK-HPV slipper and counter disk

The EDX spectra peaks are semiquantitative, showing elemental presence. Calculated weight percentages are shown besides. Gold peaks originate from sputter coating for conductivity. All polymer slippers contain carbon and oxygen as main PEEK elements (hydrogen cannot be detected), with negligible compositional change during testing, as a thin graphite/PTFE layer forms already during lapping. Minor silicon traces may indicate reactions with silicone-based antifoam additives. On the 100Cr6 counter surfaces, increased carbon content after testing shows the formation of a transfer film. By locally dissolved measurements a continuous graphite/PTFE-based film could be confirmed, providing a stable, low-wear behavior in the slipper contact.

4. DISCUSSION

To explain the pressure-dependent behavior and differences between NFM and polymer slippers, leakage and hydrostatic relief were numerically evaluated using Eqs. (1.1)–(1.6) and (1.10)–(1.12) for deformed gaps with logarithmic (Eq. (1.7)) and polynomial (3rd- and 5th-order, Eqs. (1.8) (poly3), (1.9) (poly5) profiles based on simulated deformations from [3]. Fig. 4.1 shows the NFM and PEEK-CF30 gap geometries (left), the pressure dependence of the poly5 gap (center), and the resulting pressure profiles (right).

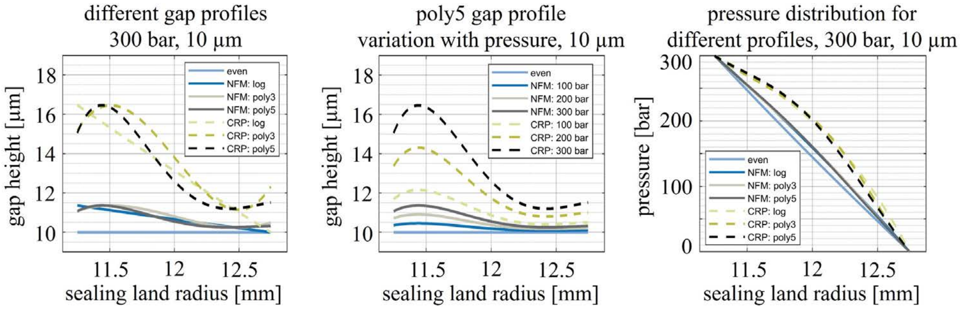

Figure 4.1: Comparison of pressure distributions for different gap profiles

The lower stiffness of polymers (NFM 80 GPa; natural PEEK 4.3 GPa; PEEK-HPV 5.9 GPa; PEEK-CF30 7.7 GPa) leads to significant pressure-dependent deformation, which enlarges the high-pressure area and shifts the hydrostatic pressure drop outward. This reduces flow conductance and leakage while increasing the hydrostatic relief (Fig. 4.2).

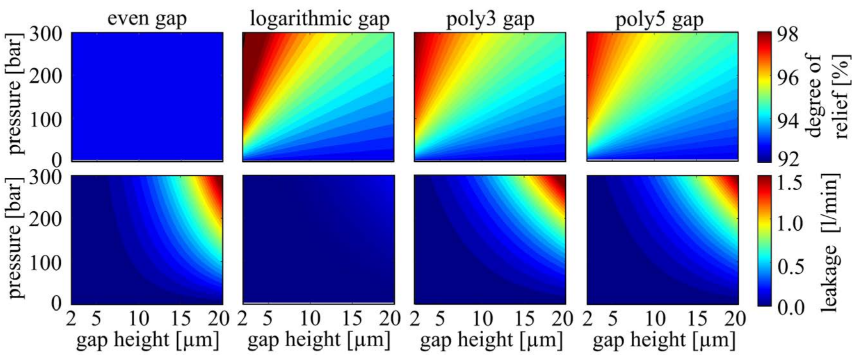

Figure 4.2: Influence of gap profile for PEEK-natural

Fig. 4.2 shows that the logarithmic gap poorly fits the measured leakage (Fig. 3.3), while the poly5 profile agrees reasonably. Moreover, for natural PEEK, the calculated hydrostatic relief deviates by up to 4.9 % at 300 bar and a 2 µm gap. Fig. 4.3 summarizes deviations for all materials: ≤ 2.2 % for NFM and up to 4.5 % for PEEK-CF30.

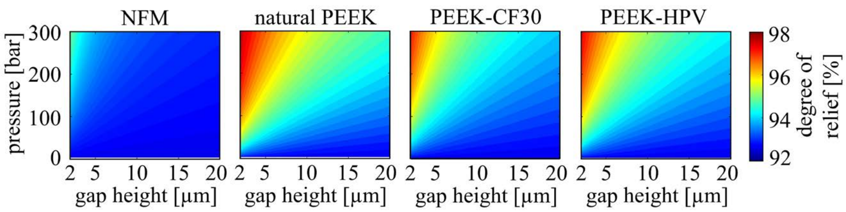

Figure 4.3: Comparison of relief change for different materials

Although approximate, these results highlight the deformation effects relevant for interpreting Sec. 3. Accurate relief design requires precise elastohydrodynamic (EHL) analysis. At 10 µm and 200 bar, PEEK-CF30 shows a 1.3 % higher relief than NFM, leading to 19 % lower residual load. Consequently, wear and friction coefficients become less comparable. Due to higher gaps and lower residual load, the transition to full-film lubrication shifts to lower speeds. The calculated leakage of PEEK-CF30 is 36 % higher than for NFM, indicating that surface non-flatness contributes at least similarly to leakage deviation. In summary, deformation effects can explain the measured results. While moderate deformation can be beneficial by enhancing pressure-dependent relief and reducing friction and wear, excessive elasticity, as seen for natural PEEK, renders the material unsuitable. Therefore, reinforced polymers are required, and uneven deformation must be prevented by geometric design adjustments to avoid non-uniform wear or early sealing land failure. Moreover, a precise lapping process is necessary to achieve even running surfaces.

5. CONCLUSION AND OUTLOOK

This study experimentally evaluated the potential of high-performance PEEK-based polymers to replace non-ferrous metals (NFM) in the slipper–swashplate contact of axial piston machines using a single-piston test rig. Polymer slippers showed a stronger pressure dependence due to deformation, making stiff grades such as PEEK-CF30 most suitable. PEEK-CF30 exhibited up to 43 % lower friction at low speeds and up to 48 % higher friction at higher speeds, the latter caused by increased fluid friction from higher manufacturing-related leakage. Leakage exceeded the NFM reference pressure dependent by about 26–185 %, yet remained small relative to the pump flow, yielding total efficiencies above 95 %, only about 1 % lower than NFM. The wear coefficient of PEEK-CF30 ($5.9 \cdot 10^{-10}$ mm³/Nm) is slightly higher, but in the same order of magnitude as NFM. SEM analysis revealed two-body abrasion as the main wear mechanism, with no thermal or chemical degradation, while EDX confirmed a thin transfer film, ensuring stable low friction and wear. Optical wear analysis indicated that the tested geometry is unsuitable for polymers due to excessive, asymmetric deformation. It can therefore be concluded that polymer slippers are feasible for use in axial piston machines, provided that geometric adaptations compensate deformation.

Future work will investigate PEEK-CF30 slippers with optimized geometry on the same test rig to quantify deformation compensation and achieve uniform wear for long-term operation.

Subsequently, full-machine tests will evaluate the efficiency and durability of pumps equipped entirely with polymer slippers.

6. ACKNOWLEDGEMENT

This work was created within the project "Improvement of oil-hydraulic polymer slippers using a physically based transient design method" (funding code 531424256) funded by the German Research Foundation DFG. The authors want to thank the DFG for this support.

7. REFERENCES

[1] N. D. Manring, 'Fluid Power Pumps & Motors: Analysis, Design, and Control', 1st ed. New York, USA: McGraw-Hill Education, 2013, ISBN: 978-0-07-181220-7.

[2] M. Ivantysynova and J. Ivantysyn, 'Hydrostatic Pumps and Motors: Principles, Design, Performance, Modeling, Analysis, Control and Testing', 1st ed. New Delhi, India: Tech Books International, 2003, ISBN: 81-88305-08-1.

[3] F. Schlegel, K. Schmitz, 'Geometric design of axial piston machine slipper-bearings made of high-performance plastics', Engineering Research, vol. 89, no. 26, 2025, https://doi.org/10.1007/s10010-025-00813-2.

[4] B. Reetz and T. Münch, 'Challenges of novel lead-free alloys in hydraulics', in Proc. 12th Int. Fluid Power Conf., vol. 1, pp. 17–25, Technische Universität Dresden, Dresden, Germany, 2020, https://doi.org/10.25368/2020.9

[5] J. Stryczek, M. Banaś, and J. Krawczyk, 'The fluid power elements and systems made of plastics', Procedia Engineering, vol. 176, pp. 600–609, 2017, https://doi.org/10.1016/j.proeng.2017.02.303.

[6] M. Rokala, 'Analysis of Slipper Structures in Water Hydraulic Axial Piston Pumps', Doctoral thesis, Tampere Univ. of Technology, Publ. 1055, Tampere, Finland, 2012, https://urn.fi/URN:ISBN:978-952-15-2872-9.

[7] F. Schoemaker, H. Murrenhoff, 'Piston Slippers for Robust Water Hydraulic Pumps', Proceedings of the 11th Int. Fluid Power Conf. Vol1, pp.236-247, RWTH Aachen University, Aachen, 2018, https://doi.org/10.18154/RWTH-2018-224460.

[8] Z. Guan et al., 'Friction and wear characteristics of CF/PEEK against 431 stainless steel under high hydrostatic pressure water lubrication', Materials & Design, vol. 196, art. no. 109057, 2020, https://doi.org/10.1016/j.matdes.2020.109057.

[9] S. Nie, F. Lou, and F. Yin, 'Tribological performance of CF-PEEK sliding against 17-4PH stainless steel with various cermet coatings for water hydraulic piston pump application', Coatings, vol. 9, no. 7, p. 436, 2019, https://doi.org/10.3390/coatings9070436.

[10] D. Li et al., 'Difference in tribological characteristics between CFRPEEK and stainless steel under water lubrication in friction testing machine and axial piston pump', *Lubricants*, vol. 11, no. 4, p. 158, 2023, https://doi.org/10.3390/lubricants11040158.

[11] F. Schlegel et al., 'Swelling, wear and property changes of high-performance polymers in oil-hydraulic tribological contacts', TuS, vol. 72, no. 1, 2025, https://doi.org/10.24053/TuS-2025-0002.

[12] F. Schlegel, A. Merkel, K. Schmitz, 'Experimental and simulative Investigation of a partially hydrostatic relived contact in variable speed axial piston machines', TuS, vol. 70. No. 4+5, 2025, https://doi.org/10.24053/Tus-2023-0023

Biographies

Felix Schlegel received his bachelor's degree in 2020 and his masters degree in 2022 from RWTH Aachen University. For his master's thesis on slippers in high-speed axial piston pumps, he was awarded by the German Society for Tribology. Since 2023, he has been a research associate at the Institute for Fluid Power Drives and Systems (ifas), focusing on tribology of piston pums, and assumed leadership of the tribology group in May 2025. His current doctoral research investigates polymer slippers using several experimental test rigs and electrohydrodynamic simulations.

Prof. Katharina Schmitz studied mechanical and chemical engineering at RWTH Aachen University and Carnegie Mellon University, Pittsburgh (USA) and graduated 2015 as Dr.-Ing. at RWTH Aachen University. Since 2018, she is full professor at RWTH Aachen University and director of the Institute for Fluid Power Drives and Systems (ifas). In addition, she is Vice Dean of the Faculty for Mechanical Engineering at RWTH Aachen, a position she holds since 2020. Prof. Schmitz's awards and honors include several best paper awards and 2023 IMechE Joseph Bramah Medal award.